Journal of Power Sources 195 (2010) 2806–2809

Contents lists available at ScienceDirect

Journal of Power Sources

journal homepage: www.elsevier.com/locate/jpowsour

Short communication

Cell resistances of poly(2,5-benzimidazole)-based high temperature polymer membrane fuel cell membrane electrode assemblies: Time dependence and influence of operating parameters

K. Wippermann*, C. Wannek, H.-F. Oetjen, J. Mergel, W. Lehnert

Institute of Energy Research – Fuel Cells (IEF-3), Forschungszentrum Jülich GmbH, Helmholtzring, 52425 Jülich, Germany

ARTICLE INFO

Article history:
Received 19 June 2009
Received in revised form 2 October 2009
Accepted 21 October 2009
Available online 13 November 2009

Keywords:
ABPBI
Cell resistance
HT-PEFC
Impedance
PBI
Phosphoric acid

ABSTRACT

Time-dependent measurements of cell impedance of a HT-PEFC based on ABPBI were performed at constant frequencies close to the high-frequency (h.f.) intercept of the corresponding Nyquist plots with the real axis. The h.f. impedances approximate the ohmic resistance of the cell and they decrease, when current (140 mA cm^{-2}) is switched on. Steady-state values are attained after 10 min. *Vice versa*, when current is switched off (OCV), the h.f. impedances instantaneously increase but reach steady-state values only after about 1 h. These values rise with increasing gas flow rates. The results are discussed in terms of hydration/dehydration processes, changing the equilibrium between orthophosphoric and pyrophosphoric acid and thus the conductivity of the electrolyte as well as the mobility of molecules and charge carriers. Impedance spectra were recorded after each time-dependent measurement under OCV conditions. The fit of these impedance data based on an equivalent circuit revealed ohmic resistances corrected by h.f. inductances and low frequency impedances associated with the cathode oxygen exchange reaction. The charge transfer resistances deduced from the low frequency impedances strongly depend on both air and hydrogen flow rates.

1. Introduction

Polymer electrolyte fuel cells (PEFCs) with significantly higher working temperatures than 100 °C do not require high-purity hydrogen as fuel, and therefore they are beneficial for devices that run on hydrogen produced on-site by reforming of hydrocarbon energy carriers, e.g. in the field of mobile and stationary applications where middle distillates (kerosene, diesel, fuel oil) can be used to provide the necessary hydrogen.

Most of today's high temperature cells (HT-PEFCs) rely on membrane electrode assemblies (MEAs) with phosphoric acid absorbed in PBI (=*poly*(2,2′-(*m*-phenylene)-5,5′-bibenzimidazole)) as electrolyte [1]. Recently membranes based on the chemically related ABPBI (=*poly*(2,5-benzimidazole)) have emerged as a promising alternative [2–4].

Various aspects of the steady-state cell impedance of HT-PEFCs based on PBI as membrane polymer at different operating conditions have already been reported in the literature (e.g. [5–7]). The influence of water activity on the steady-state conductivity of the electrolyte [8,9] as well as the distribution of phosphoric acid within the membrane electrode assembly (MEA) [10,11] are intensively studied at present.

We will not only discuss the influence of several testing parameters on the cell resistance of a MEA based on ABPBI instead of PBI, but we will also turn our attention to its time dependence after changes of the operating conditions.

2. Experimental

MEAs (A = 14.4 cm^2) have been assembled from ABPBI membranes (FuMA-Tech) and gas diffusion electrodes (~1 mg Pt cm^{-2}) produced in-house which have been impregnated with appropriate amounts of phosphoric acid [4]. Except the experiments with humidified hydrogen, where MEAs with 26 μm thin ABPBI membranes were used, all studies were performed with MEAs including 38 μm thin ABPBI membranes. They have been characterized in a single cell using pure hydrogen and air at ambient pressure as the reactants. Under these conditions reasonable power densities of ~250 mW cm^{-2} are obtained at T = 160 °C [4].

We have deduced the time-dependent ohmic resistances from impedance measurements using a symmetric two-electrode configuration. The experiments were run at a predefined frequency of 5–10 kHz close to the high-frequency intercept of the corresponding Nyquist plots with the real axis. The advantage of such

* Corresponding author. Tel.: +49 2461 612572; fax: +49 2461 616695.
E-mail address: k.wippermann@fz-juelich.de (K. Wippermann).

0378-7753/$ – see front matter © 2009 Elsevier B.V. All rights reserved.
doi:10.1016/j.jpowsour.2009.10.100

Table 1
Ohmic and charge transfer resistances obtained from impedance measurements (see Figs. 1, 2, 4 and 5).

$\lambda_{air}/\lambda_{H_2}$	Final value of time-dependent h.f. impedance values at constant frequency ('ohmic resistance'): Re(Z) @ Im ≈ 0/mΩ cm^2	Impedance spectra: Re(Z) @ Im = 0/mΩ cm^2	Fit of impedance spectra: R_Ω/mΩ cm^2, fit code: $R_\Omega L(R_2Q_2)(R_3Q_3)(R_{ct}Q_4)$	Fit of impedance spectra: R_{ct}/mΩ cm^2
2/2	272	272	248	3010
4/2	289	288	252	4360
4/4	306	307	263	4020
6/2	311	307	267	6440
6/6	333	336	289	5360

single-frequency experiments is the high time resolution of 5 s per point. However, disturbances caused by high-frequency inductances have to be considered (see below). Before each measurement the MEA was run overnight with j = 200 mA cm^{-2} at T = 160 °C with hydrogen and air at flow rates corresponding to the stoichiometric factors $\lambda_{Cathode/Anode}$ = 2/2, only interrupted by the recording of 2 polarization curves. Exactly 2 h prior to the beginning of the time-dependent measurements during which the current density was changed from j = 0 to 140 mA cm^{-2} and *vice versa* at 160 °C the cell was switched to OCV and the hydrogen and air flow rates were changed to the values used for the respective experiment (λ_{air} = 2/4/6, λ_{H_2} = 2/4/6). In case of OCV measurements, the indicated air and hydrogen stoichiometries refer to the corresponding flow rates at a current density of 140 mA cm^{-2}. During time-dependent measurements, the phase angle of the impedance at constant frequency varied in the range of −3° to +3°. This deviation results in a small error of the measured impedance of ±2% (see Table 1 , comparison of data in columns no. 2 and 3).

A more serious source of error is the high-frequency inductance. In order to eliminate this error, impedance spectra were performed additionally after the end of each time-dependent experiment in a frequency range of 10^{-2}–10^4 Hz under OCV steady-state conditions. The AC signal voltage amplitude was always ±10 mV. The impedance spectra were fitted on basis of an equivalent circuit (see Fig. 3) using the EQUIVCRT 3.0 Software written by Boukamp [12]. From the fit data, corrected data of the ohmic resistance, R_Ω, could be obtained. In the following, the original impedance values will be denoted as R'_Ω ('ohmic resistance') and the corrected fit data of the ohmic resistance will be indicated as R_Ω. All the impedance measurements were performed with an IM 6 unit of Zahner Elektrik.

3. Results and discussion

After changing the operating parameters of a HT-PEFC MEA it takes several minutes up to a few hours before the ohmic resistance reaches a steady state. This is particularly the case when the current density is changed. While at OCV ohmic resistances of 250–300 mΩ cm^2 have been observed, these values drop down within a few minutes to about 200 mΩ cm^2 when current is drawn from the cell.

Fig. 1 shows the time-dependent behaviour of the 'ohmic resistance', more precisely the high-frequency impedance at constant frequency at Im(Z) part of almost zero, for three different air flow rates. The initial values of 250–300 mΩ cm^2 under OCV conditions drop down within 10 min to about 200 mΩ cm^2 when a current density of 140 mA cm^{-2} is switched on. The 'ohmic resistance' reaches steady-state values, which shows only a weak dependence on the air flow rate. These results can be explained by the production of water in the cathode, which increases the conductivity of the electrolyte by increasing the amount of free phosphoric acid compared to its less conductive dehydration products (mainly pyrophosphoric acid $H_4P_2O_7$) [13] in the electrodes (especially the cathode) and the membrane.

After 3 h of operation, the current was turned off. The instantaneous increase of the 'ohmic resistances' indicates a more or less reversible hydration/dehydration process. Indeed, it takes the resistances about 1 h, to reach steady-state values during the dehydration process under OCV conditions. A simple explanation for the much faster hydration process is the *in situ* water production at the cathode, compared to the slow removal of water by diffusion processes in case of dehydration process. Moreover, the water uptake of both orthophosphoric and pyrophosphoric acid is a fast process due to their hygroscopic nature. Similarly, rapid water uptake but slow water removal has been observed by Daletou et al. during thermogravimetrical experiments on free-standing acid-doped HT-PEFC membranes [8]. The steady-state values of the 'ohmic resistances' under OCV conditions exhibit a significant increase

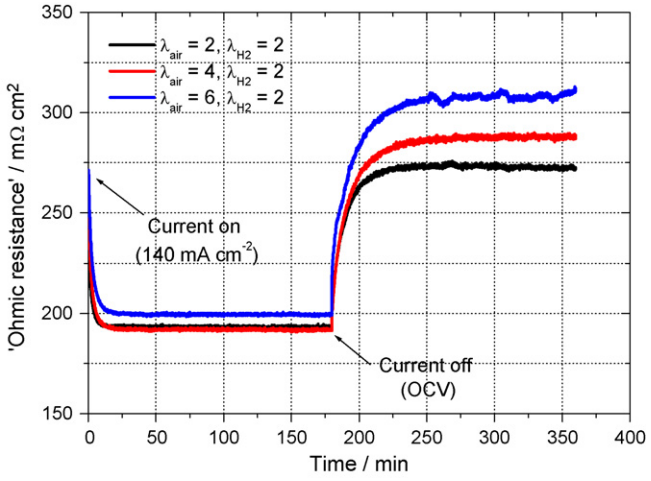

Fig. 1. Time dependence of the cell resistance after changing the current density from j = 0 to 140 mA cm^{-2} and *vice versa* at 160 °C; variation of λ_{air} = 2/4/6; λ_{H_2} = 2 (constant).

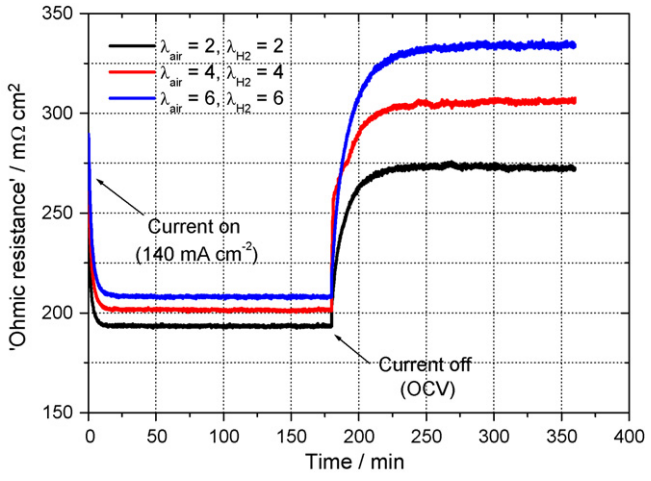

Fig. 2. Time dependence of the cell resistance after changing the current density from j = 0 to 140 mA cm^{-2} and *vice versa* at 160 °C; variation of $\lambda_{air} = \lambda_{H_2}$ = 2/4/6.

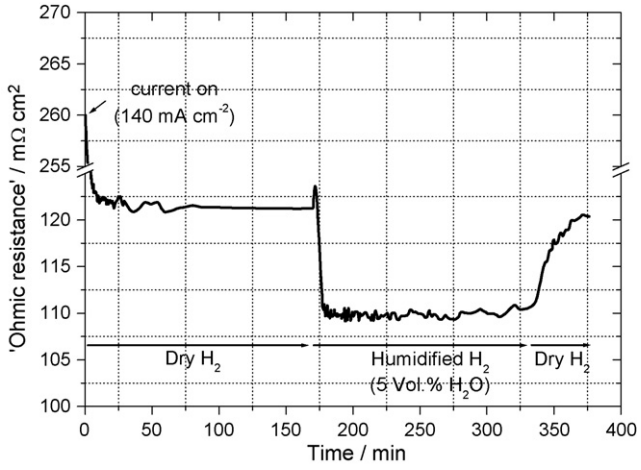

Fig. 3. Reversible change of the cell resistance depending on the humidity of hydrogen gas (0/5%); $j = 140\,mA\,cm^{-2}$, $T = 160\,^{\circ}C$.

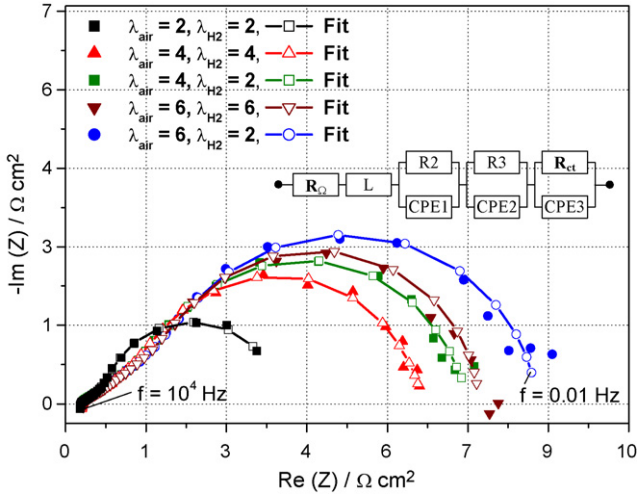

Fig. 4. Nyquist plots of the MEA impedance under OCV conditions; $T = 160\,^{\circ}C$; variation of $\lambda_{air}/\lambda_{H_2}$; measured values: closed symbols, fit values: lines and open symbols; frequency range: 10^{-2}–10^{4} Hz; AC amplitude: 10 mV.

with rising air flow rate. This effect is even more pronounced if hydrogen flow rate is also enhanced (see Fig. 2). These results are consistent with the idea of a dehydration process, which should be promoted by increased gas flow rates at both electrodes.

On the long term, after complete dehydration of the cell, one would expect a coincidence of the values of the 'ohmic resistances'. In this case, our 'final' values of the 'ohmic resistances' would represent a snap-shot in a very slow process. However, due to non-negligible hydrogen and oxygen permeation through the membrane and a subsequent, continuous production of water within the MEA, a complete dehydration of the cell seems to be improbable, as long as electrodes are supplied by hydrogen respectively air. In the published literature there has been considerable debate about the values measured for the gas permeabilities of acid-doped PBI-type membranes, and some authors deny their relevance to the fuel cell behaviour (e.g. [8,14]). Nevertheless, the values given by He et al. [15] for doped PBI at 180 °C are 25–30 times as high as those observed with Nafion at 80 °C, and from Fig. 7 in [16] it could be deduced that the loss current density due to hydrogen permeation for a highly doped PBI membrane operated at $T = 150\,^{\circ}C$ is in the order of 5–10 mA cm^{-2}. This competition between hydration by permeating gases and dehydration of the MEA by the different gas flows may explain the 'ohmic resistances' reaching different steady-state values during dehydration process. The comparatively small effect of the flow rates during current flow can be explained by a 'weakening' effect because of water production in the cathode.

Generally, the hydration/dehydration process should influence the local equilibrium between free phosphoric acid and its dehydration products in the electrodes and the membrane and thus have impact on local physico-chemical properties of the HT-PEFC such as proton conductivity, active catalyst surface and gas permeability of the membrane. For example, if a current is drawn from the cell, water is produced at the cathode and a concentration profile of the water activity across the MEA is generated. Because the amount of mobile H_3PO_4 is enhanced by an increasing local water activity, phosphoric acid should move from the anode to the cathode under current flow and *vice versa*, if current is switched off. This effect should have a pronounced effect on the local ratio of orthophosphoric and pyrophosphoric acid and thus local physico-chemical properties like proton conductivity, gas permeability and the active surfaces of the electrodes.

Besides current density and gas flow rates, cell temperature and humidity of supplied gases should play an important role in the hydration/dehydration process. A first measurement with humidified fuel gas is shown in Fig. 3. Starting the experiment with dry hydrogen gas, a constant resistance of 121 mΩ cm^2 is reached at about ten minutes after switching on the current. The resistance is only about 60% of that obtained in the previous experiments (see Figs. 1 and 2). This is mainly due to the lower thickness of the ABPI membrane used in the humidification experiment (26 μm instead of 38 μm). When starting the humidification of hydrogen gas (5 vol.% H_2O in H_2) it takes only seven minutes until the cell resistance drops to a constant value of 110 mΩ cm^2. After stopping the humidification of fuel gas, it takes about half an hour until the initial value of cell resistance is re-established. This result supports again our reasoning based on a reversible hydration/dehydration process. In future experiments, the influence of these parameters has to be investigated in more detail.

After each time-dependent measurement, impedance spectra were recorded under OCV conditions in the frequency range of 0.01 Hz to 10 kHz. Figs. 4 and 5 show Nyquist plots of the MEA impedance at different flow rates of air and hydrogen. The indicated air and hydrogen stoichiometries refer to the corresponding flow rates at a current density of 140 mA cm^{-2}. Measured values are marked by closed symbols and fit data are indicated by lines and

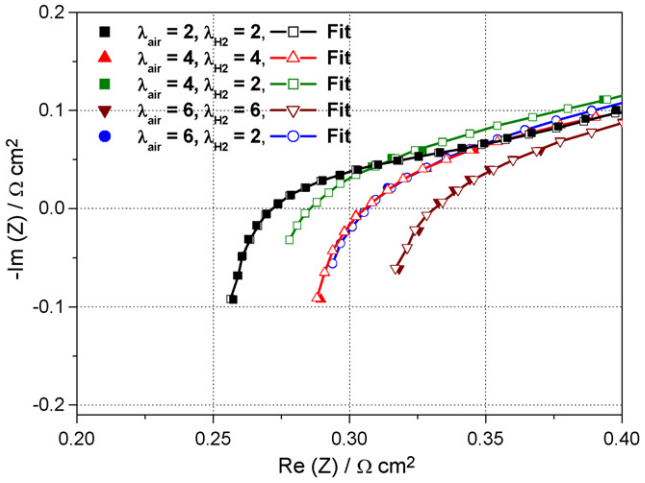

Fig. 5. Enlarged view of the high-frequency impedances shown in the Nyquist plots in Fig. 4.

open symbols. The fit values were obtained by using the equivalent circuit shown in Fig. 4. The measured values and selected fit data are summarized in Table 1.

R_Ω is the sum of membrane resistance, the ohmic resistance of the electrodes, contact resistances and other ohmic contributions. The columns 2–4 of Table 1 compare three different values of ohmic resistance dependent on the gas flow rates: (i) final value of time-dependent h.f. impedance values at constant frequency, so-called 'ohmic resistance', R'_Ω (see Figs. 1 and 2), (ii) real part of impedance for $\mathrm{Im}(Z)=0$ (see Fig. 5), (iii) fit value R_Ω based on the equivalent circuit shown in Fig. 4. Because the values of (i) and (ii) are almost identical, it is evident that the small deviation of phase angle from zero during the course of time-dependent measurements (see Section 2) can be neglected. The fit values R_Ω (iii) are about 10% smaller than those of R'_Ω, because the high-frequency inductance is taken into account. Insofar, R_Ω reflects the true ohmic resistance of the cell. However, the dependence on the gas flow rates is the same.

The high-frequency (h.f.) inductance, L, is mainly due to artefacts originating from the cables and the measuring device. The h.f. elements, R1, CPE1 (CPE = constant phase element), R2 and CPE2 have no physical meaning. They simply describe the linear slope of the spectra at high frequencies. Such behaviour can be explained by a dominating proton transport and double layer charging in the h.f. part caused by the mixed (proton + electron) conductivity of the electrodes (see e.g. [17–21]). The 40° angle of the straight lines is close to the predicted value of 45°. In future work, we will calculate the proton conductivities of the HT-PEFC electrodes from the h.f. linear part of the impedance spectra considering the 'transmission line' model [17].

In a first approximation, limiting mass transport processes under OCV conditions and limitation of hydrogen reaction rate can be neglected. Under these assumptions, the large semi-arc at medium and low frequencies (see Fig. 4) is mainly attributed to the charge transfer resistance, R_{ct}, of the oxygen exchange reaction. If air flow rate is enhanced ($\lambda=2$ to $\lambda=6$) at constant hydrogen flow rate ($\lambda=2$), R_{ct} increases from 3.0 to 6.4 $\Omega\,cm^{-2}$ (see Table 1 and Fig. 4). Interestingly, this effect is slightly diminished, if hydrogen flow is also increased, i.e. hydrogen and air stoichiometries are equal: In this case, R_{ct} increases from 3.0 to only 5.4 $\Omega\,cm^{-2}$ (see Table 1 and Fig. 4).

On basis of the results presented here, the following tentative explanation may be given: If air flow rate is increased, the water content of the MEA decreases and the amount of pyrophosphoric acid in the equilibrium between $2H_3PO_4 - H_4P_2O_7 + H_2O(g)$ increases. For this reason, the proton conductivity of the MEA decreases, causing a decrease of catalytic activity especially in the outer part of the cathode. Because the solubility of oxygen in H_3PO_4 is much lower than in water [22], the oxygen concentration nearby the platinum catalyst decreases, in spite of the higher air flow rate. Both effects decrease the exchange current density of the oxygen equilibrium reaction and thus increase the charge transfer resistance, R_{ct}, as observed.

By increasing the hydrogen flow rate, more hydrogen permeates from the anode through the membrane to the cathode. Although hydrogen 'consumes' a part of the oxygen which is present at the cathode, the increased formation of water causes a much better solubility of oxygen and a more thorough wetting of the inner surface of catalyst layer, leading to an enhanced oxygen concentration respectively a higher activity of the cathode. Hence, the exchange current density of the oxygen equilibrium reaction increases and R_{ct} decreases.

4. Conclusions

It turns out, that time-dependent measurements of cell impedance at different operating conditions are crucial since they provide a valuable insight into the hydration/dehydration processes of HT-PEFCs. We attribute the fact that high water production by the fuel cell reaction, high water insertion and its low removal by the gas flows (i.e. the water content in the cell) lowers the ohmic resistance to the increasing amount of mobile H_3PO_4 in the electrolyte. The hydration process is fast because of the water production inside the cathode, compared to the slow removal of water by diffusion processes through the gas diffusion layer into the channel. In general, ohmic resistances become small when (i) the current density is increased, (ii) the gas flows are reduced, (iii) the cell is run at elevated temperatures and (iv) when the fuel gas is humidified.

Furthermore, the hydration/dehydration processes are believed to influence the local distribution of free phosphoric acid in the cell and thus local physico-chemical properties of the HT-PEFC, like proton conductivity, oxygen gas solubility and inner active surface of the electrodes. For future studies, it is therefore important to investigate the local distribution and composition of the phosphoric acid electrolyte depending on the operation conditions of HT-PEFC in more detail.

Acknowledgement

We thank Matthias Prawitz for performing the impedance measurements.

References

[1] J. Mader, L. Xiao, T.J. Schmidt, B.C. Benicewicz, Adv. Polym. Sci. 216 (2008) 63–124.
[2] J.A. Asensio, P. Gómez-Romero, Fuel Cells 5 (2005) 336–343.
[3] C. Wannek, B. Kohnen, H.-F. Oetjen, H. Lippert, J. Mergel, Fuel Cells 8 (2008) 87–95.
[4] C. Wannek, W. Lehnert, J. Mergel, J. Power Sources 192 (2009) 258–266.
[5] N.H. Jalani, M. Ramani, K. Ohlsson, S. Buelte, G. Pacifico, R. Pollard, R. Staudt, R. Datta, J. Power Sources 160 (2006) 1096–1103.
[6] Y. Tang, J. Zhang, C. Song, J. Zhang, Electrochem. Solid-State Lett. 10 (2007) B142–B146.
[7] J. Lobato, P. Canizares, M.A. Rodrigo, J.J. Linares, Electrochim. Acta 52 (2007) 3910–3920.
[8] M.K. Daletou, J.K. Kallitsis, G. Voyiatzis, S.G. Neophytides, J. Membr. Sci. 326 (2009) 76–83.
[9] A. Schechter, R.F. Savinell, J.S. Wainright, D. Ray, J. Electrochem. Soc. 156 (2009) B283–B290.
[10] K. Kwon, T.Y. Kim, D.Y. Yoo, S.-G. Hong, J.O. Park, J. Power Sources 188 (2009) 463–467.
[11] C. Wannek, I. Konradi, J. Mergel, W. Lehnert, Int. J. Hydrogen Energy 34 (2009) 9479–9485.
[12] B.A. Boukamp, Equivalent Circuit, Internal Report CT89/214/128, University of Twente, 1989.
[13] Z. Liu, J.S. Wainright, M.H. Litt, R.F. Savinell, Electrochim. Acta 51 (2006) 3914–3923.
[14] S.C. Kumbharkar, M.N. Islam, R.A. Potrekar, U.K. Kharul, Polymer 50 (2009) 1403–1413.
[15] R. He, Q. Li, A. Bach, J.O. Jensen, N.J. Bjerrum, J. Membr. Sci. 277 (2006) 38–45.
[16] Y. Oono, A. Sounai, M. Hori, J. Power Sources 189 (2009) 943–949.
[17] R. de Levie, in: P. Delahay, C. Tobias (Eds.), Advances in Electrochemistry and Electrochemical Engineering, Vol. 6, Interscience Publishers, New York, 1967, p. 360.
[18] M. Eikerling, A.A. Kornyshev, J. Electroanal. Chem. 475 (1999) 107–123.
[19] Y. Bultel, L. Genies, O. Antoine, P. Ozil, R. Durand, J. Electroanal. Chem. 527 (2002) 143–155.
[20] A. Havránek, K. Wippermann, J. Electroanal. Chem. 567 (2004) 305–315.
[21] L. Birry, C. Bock, X. Xue, R. McMillan, B. MacDougall, J. Appl. Electrochem. 39 (2009) 347–360.
[22] K. Klinedinst, J.A.S. Bett, J. MacDonald, P. Stonehart, J. Electroanal. Chem. 57 (1974) 281–289.